

Retinex Meets Language: A Physics-Semantics-Guided Underwater Image Enhancement Network

Shixuan Xu, Yabo Liu, Junyu Dong, *Member, IEEE*, and Xinghui Dong, *Member, IEEE*

Abstract—Underwater images often suffer from severe degradation caused by light absorption and scattering, leading to color distortion, low contrast and reduced visibility. Existing Underwater Image Enhancement (UIE) methods can be divided into two categories, i.e., prior-based and learning-based methods. The former rely on rigid physical assumptions that limit the adaptability, while the latter often face data scarcity and weak generalization. To address these issues, we propose a Physics-Semantics-Guided Underwater Image Enhancement Network (PSG-UIENet)¹, which couples the Retinex-grounded illumination correction with the language-informed guidance. This network comprises a Prior-Free Illumination Estimator, a Cross-Modal Text Aligner and a Semantics-Guided Image Restorer. In particular, the restorer leverages the textual descriptions generated by the Contrastive Language-Image Pre-training (CLIP) model to inject high-level semantics for perceptually meaningful guidance. Since multimodal UIE data sets are not publicly available, we also construct a large-scale image-text UIE data set, namely, LUIQD-TD, which contains 6,418 image-reference-text triplets. To explicitly measure and optimize semantic consistency between textual descriptions and images, we further design an Image-Text Semantic Similarity (ITSS) loss function. To our knowledge, this study makes the first effort to introduce both textual guidance and the multimodal data set into UIE tasks. Extensive experiments on our data set and four publicly available data sets demonstrate that the proposed PSG-UIENet achieves superior or comparable performance against fifteen state-of-the-art methods.

Index Terms—Underwater Image Enhancement (UIE), Retinex Theory, CLIP, Image-Text Fusion, Multimodal Underwater Data.

I. INTRODUCTION

UNDERWATER images play a critical role in a diverse range of applications, including marine biology research, underwater archaeology, seabed mapping, and autonomous robot navigation. However, the unique optical properties of water—characterized by absorption, scattering, and suspended particles—inevitably degrade image quality. As a result, underwater images often suffer from severe artifacts, such as color distortion, low contrast, and reduced visibility. These

This study was supported in part by the National Natural Science Foundation of China (NSFC) (No. 42576200) and in part by the Key Research and Development Program of Shandong Province, China (No. 2024ZLGX06)(Corresponding author: Xinghui Dong).

S. Xu, Y. Liu, J. Dong and X. Dong are with the State Key Laboratory of Physical Oceanography and the Faculty of Information Science and Engineering, Ocean University of China, Qingdao, 266100. (e-mail: xushixuan@stu.ouc.edu.cn, yaboliu.ug@gmail.com, dongjunyu@ouc.edu.cn, xinghui.dong@ouc.edu.cn).

¹The data set, source code and model will be made publicly available at <https://github.com/INDTLab/PSG-UIENet> upon the acceptance of the paper.

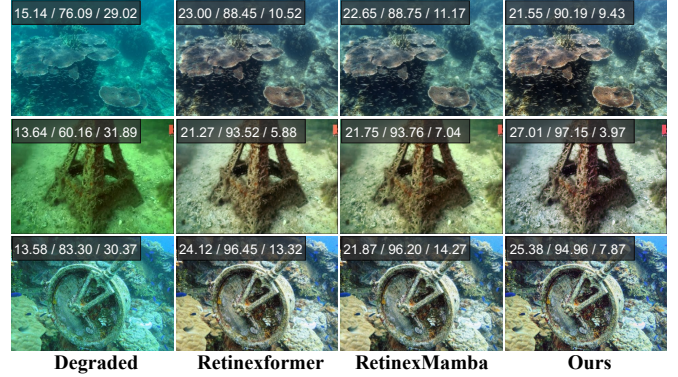


Fig. 1. Comparison of three Retinex-based UIE methods, including Retinexformer [17], RetinexMamba [18], and our PSG-UIENet. In terms of each image, the PSNR, SSIM [19], and LPIPS [20] values computed between the corresponding reference image and it are shown at the top-left corner. These results highlight the effectiveness of the Retinex theory [21] in alleviating underwater image degradation.

degradations will impair the reliability of both manual analysis and automated systems, becoming a major bottleneck of underwater exploration and monitoring tasks. Therefore, Underwater Image Enhancement (UIE) has emerged as a crucial research topic with significant scientific and practical values.

Many UIE methods have been developed over the years. Existing UIE methods can generally be categorized into two paradigms, i.e., prior-based and learning-based approaches. Prior-based methods [1]–[8] normally rely on handcrafted physical priors or models to estimate illumination and transmission. These methods are interpretable and computationally efficient. However, they often fail to generalize across diverse underwater environments due to their reliance on strict assumptions, which may not hold under varying conditions.

On the other hand, learning-based methods [9]–[16] generally leverage deep neural networks to directly learn complex mappings from data. For instance, Convolutional Neural Network (CNN)-based methods extract local hierarchical features to enhance degraded images, while Transformer-based approaches employ self-attention mechanisms to capture long-range dependencies. Although remarkable progress has been made, they are heavily dependent on large-scale annotated data sets. Unfortunately, existing UIE data sets normally contain limited real-world samples and lack diversity, thereby decreasing the generalization of the model trained. Thus, both paradigms face inherent limitations, underscoring the demand for more robust and adaptive UIE methods to diverse underwater environments.

In light of these limitations, recent studies have paid attention to hybrid paradigms [11], [15], [17], [18] that combine physical priors with deep learning techniques. Among these, the Retinex theory [21] has attracted significant attention due to its ability to effectively model illumination and reflectance. For example, Retinex priors were integrated into deep networks and achieved improvements in contrast, color accuracy, and structural preservation (see Fig. 1) [15], [17], [18].

Furthermore, vision–language models, such as Contrastive Language–Image Pre-training (CLIP) [22], have demonstrated exceptional potential to align visual and textual semantics, allowing high-level semantic guidance for image enhancement. These developments suggest that the joint use of physical priors and semantic information can address the limitations of traditional methods. However, most of the existing approaches [23]–[25] often fail to fully exploit the complementary strengths of the two types of data. Specifically, the scarcity of multimodal data sets severely limits the integration of physical priors and semantics-driven guidance in domain-specific tasks, e.g., underwater image enhancement. This limitation motivates us to explore a new framework that bridges the gap by leveraging both physical priors and text-based semantics.

To this end, we propose a novel Physics-Semantics-Guided Underwater Image Enhancement Network (PSG-UIENet). This network integrates physics-inspired priors obtained using the Retinex theory [21] with semantic guidance provided by textual descriptions, forming a unified multimodal enhancement framework. Specifically, PSG-UIENet consists of a Prior-Free Illumination Estimator, a Cross-Modal Text Aligner and a Semantics-Guided Image Restorer. Unlike existing Retinex-based methods [17], [18] which rely on handcrafted priors, our illumination estimator operates without fixed assumptions. The image restorer adopts a dual-branch, mask-based encoder–decoder, enabling effective integration of visual and textual features for semantically guided enhancement.

To facilitate multimodal learning, we also collect the first large-scale image–text UIE data set, i.e., LUIQD-TD. It is derived on top of the LUIQD [26] data set. In total, 6,418 image-reference-text triplets are included. Each triplet comprises a degraded image, a visually optimal reference image, and a corresponding textual description. We further propose a novel Image-Text Semantic Similarity (ITSS) loss function to explicitly enforce semantic alignment between textual descriptions and enhanced images. This loss function ensures that the enhanced image is not only visually appealing but also semantically consistent with the given textual description.

To our knowledge, this is the first study to incorporate textual descriptions into a prior-based UIE network and to build an image-reference-text data set for UIE tasks. The contributions of this study can be summarized as fourfold.

- We propose PSG-UIENet, the first physics-semantics-guided UIE network that integrates a prior-free illumination estimator and a semantics-driven image restorer, advancing multimodal UIE research.
- We construct the first multimodal UIE data set, i.e., LUIQD-TD, which contains 6,418 image-reference-text triplets, satisfying a critical demand in multimodal data for UIE tasks.

- We design a dual-branch cross-modal fusion mechanism with random pixel-level masking to extract and align textual semantics with visual features. In particular, a Cross-Attention FiLM Module (CFM) is introduced for adaptive semantic fusion.
- We perform extensive experiments on five benchmark test sets together with fifteen state-of-the-art methods. The results not only demonstrate the superiority of our approach, but also establish new baselines for future multimodal UIE research.

The rest of this paper is organized as follows. In Section II, we review the related work. Our data set is introduced in Section III. Section IV presents our method. Experimental settings and results are reported in Sections V and VI, respectively. Finally, we conclude the paper in Section VII.

II. RELATED WORK

A. Underwater Image Enhancement Methods

Underwater Image Enhancement (UIE) methods can be divided into prior-based and learning-based methods. Prior-based methods rely on physical models or handcrafted assumptions to estimate illumination or transmission, for example, Dark Channel Prior (DCP) [1], its underwater variants, i.e., UDCP [2], and GDCP [3]. Although these methods are simple and interpretable, their reliance on rigid priors often limits their adaptability to complex underwater conditions and may introduce visual artifacts [4], [27]. To address these limitations, more general priors were proposed for UIE approaches, such as Histogram Equalization (HE) [28], [29], Retinex-based methods [5], [30], and multi-exposure fusion frameworks [31], [32]. Although these approaches can improve contrast and color, they usually lack scene-awareness and struggle with handling global variations in underwater degradation [6]–[8].

In contrast, learning-based UIE approaches leverage deep neural networks to directly learn enhancement mappings from data. CNN-based [9]–[11] and Transformer-based methods [12]–[16] have demonstrated notable success by capturing local features and long-range dependencies, respectively. However, due to the scarcity of large-scale real-world underwater data sets, early models trained mainly on synthetic data suffer from domain gaps. The introduction of data sets such as UIEB [9] and SUIM-E [33] has improved model generalization by providing high-quality reference images for supervised training. Despite these advances, a small single-modal data set cannot adequately cover complex real-world underwater scenarios. In contrast, textual descriptions can leverage semantic information to compensate for the limitations of single-modal data, guiding the model toward producing more stable and perceptually-consistent enhancement results.

B. Retinex-Based Image Enhancement Methods

Inspired by the human visual system, Retinex theory [21] decomposes an image into reflectance and illumination components, providing strong physical interpretability for image enhancement tasks. Recently, this theory has been integrated with deep learning techniques to improve both interpretability and

performance. Qi et al. [15] proposed a two-stage framework that combines color correction and visibility enhancement with axial attention to better capture global context. Cai et al. [17] introduced a Transformer-based Retinex model with illumination-guided attention, effectively reducing artifacts and enhancing contrast. In [18], Bai et al. incorporated state-space modeling and illumination-fused attention into Retinex-inspired architectures, achieving improved efficiency and semantic consistency.

In contrast, the proposed PSG-UIENet advances both architecture and modeling. Specifically, we design a multi-scale illumination estimator that adaptively infers illumination without relying on handcrafted priors, thereby enhancing robustness across diverse underwater scenarios. In addition, we introduce high-level semantic cues encoded by textual descriptions, enabling context-aware enhancement that extends beyond conventional Retinex-based frameworks.

C. Text-Guided Multimodal Image Enhancement Methods

In recent years, multimodal approaches that integrate vision and language have shown great potential in image enhancement and restoration [23]–[25], [34]. Using the semantic understanding ability of pre-trained vision-language models, such as CLIP [22], these approaches aim to generate enhanced images that align more closely with human perception. In [23], CLIP-based prompt learning was introduced with a ranking optimization strategy for unsupervised backlit enhancement. Chen et al. [34] used residual vectors in the embedding space of CLIP rather than handcrafted prompts, improving the usability and transferability of CLIP guidance. In [24], CLIP guidance was applied to dehazing with region-specific prompts and contrastive learning. To bridge domain gaps between synthetic and real-world underwater images, Liu et al. [25] combined CLIP with diffusion models and a CLIP-classifier.

Nevertheless, existing text-guided methods typically treat textual input as a weak supervisory signal, relying heavily on fixed prompts or CLIP-based similarity loss functions. As a result, they cannot fully exploit the rich semantics of natural language and were mainly tailored for natural scene enhancement, leaving domain-specific tasks, e.g., UIE, largely unexplored. To address these issues, we propose a novel Physics-Semantics-Guided Underwater Image Enhancement Network (PSG-UIENet). This network explicitly integrates Retinex-inspired physical priors with semantic information encoded in textual descriptions, enabling fine-grained alignment between visual and textual modalities. Compared to existing prompt-based approaches, our method can perform robust, context-aware enhancement for challenging underwater scenarios.

III. LUQID-TD DATA SET

The availability of high-quality datasets plays a pivotal role in advancing data-driven underwater image enhancement methods. However, existing datasets face several critical limitations that hinder the development of robust and generalizable models. First, most underwater datasets are small in scale, typically containing only a few hundred samples, which restricts their utility for training deep neural networks. Second,

these datasets often lack multimodal annotations such as textual descriptions, limiting the exploration of vision–language alignment in UIE tasks. Together, these limitations underscore the pressing need for a large-scale, multimodal dataset tailored to the unique challenges of underwater image enhancement.

To mitigate the scarcity of multimodal datasets for underwater image enhancement (UIE), we extend the Large-scale Underwater Image Quality Data set (LUIQD) [26] and construct **LUQID-TD** (LUIQD with Textual Descriptions). The dataset is tailored for multimodal UIE, enabling models to jointly leverage visual content and linguistic semantics for perceptually aligned restoration and semantically guided enhancement.

A. The LUIQD Data Set

The original LUIQD data set [26] is a large-scale, human-perception-oriented benchmark developed for Underwater Image Quality Assessment (UIQA). It contains 64,180 underwater images, including 6,418 raw real-world underwater images and 57,762 enhanced images generated by a wide range of traditional and deep learning-based algorithms. Each image is annotated with a subjective quality score ranging from 0 to 100, provided by at least 20 annotators following the SS-ACR protocol and the ITU-R BT.500-12 recommendation. These annotations capture perceptual aspects such as color fidelity, contrast, texture clarity, visibility, and foreground recognition. Due to its scale, diversity, and reliable subjective scoring, the LUIQD data set serves as a solid foundation for evaluating UIE methods, selecting reference images, and constructing downstream multimodal tasks.

B. Reference Image Selection

For supervised UIE, we construct high-quality raw-reference pairs by leveraging the subjective quality scores in LUIQD. The reference images in LUQID-TD were derived from the original LUIQD data set [26]. In LUIQD, each raw underwater image is associated with nine enhanced versions produced by a set of representative traditional and deep learning-based algorithms. Each enhanced image was assigned a subjective quality score by at least 20 independent annotators following the SS-ACR protocol and ITU-R BT.500-12 recommendation. Based on these scores, we selected the enhanced image with the highest mean subjective quality as the reference image for each raw input. This standardized procedure ensures objective and reproducible reference selection. In total, we obtain 6,418 raw-reference pairs $(\mathbf{I}_i^{raw}, \mathbf{I}_i^{ref})$, providing reliable supervision for mapping degraded underwater images to their visually optimal counterparts.

C. Textual Description Annotation

To incorporate semantic information and facilitate vision–language modeling, we annotate each image pair with a natural language description T_i . These descriptions highlight the key scene elements and visual characteristics shared between the raw and reference images, including semantic content, quality attributes, and foreground–background structure.

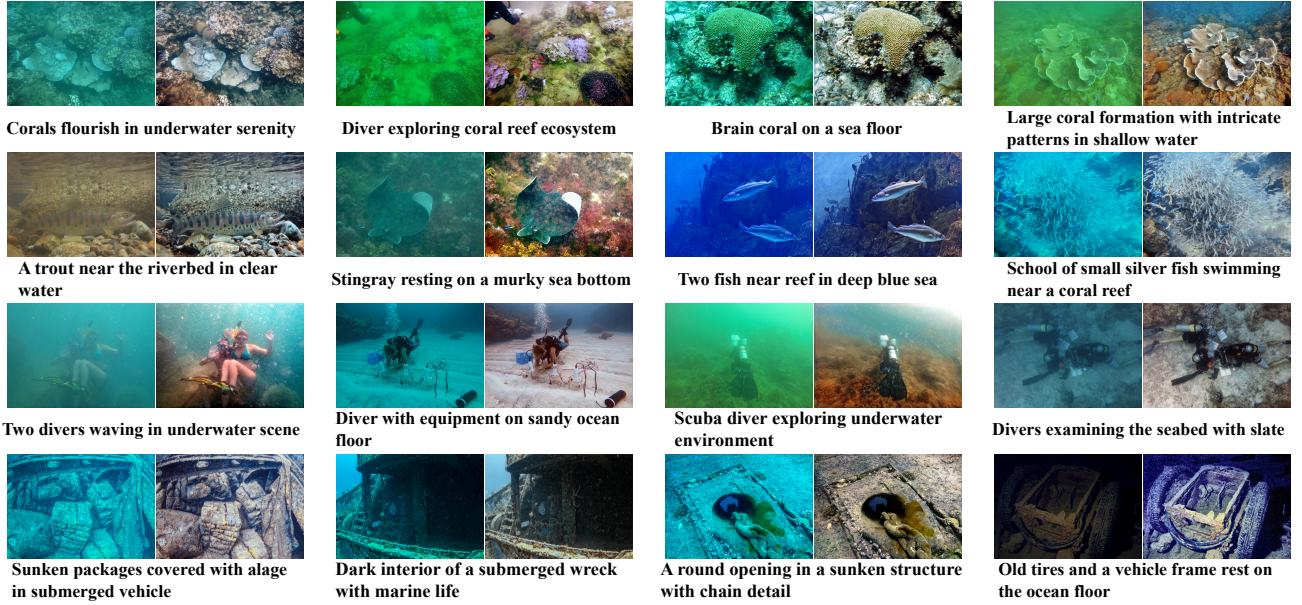


Fig. 2. Representative samples from the LUQID-TD data set. Each example consists of three components: the left image shows the raw underwater input, the right image presents the reference image with the highest perceptual quality score, and the accompanying caption provides the textual description summarizing the scene and visual attributes. The data set spans diverse underwater scenarios, including coral reefs, marine life, divers, submerged wrecks, and underwater vehicles, thereby offering rich semantic and visual information for multimodal UIE.

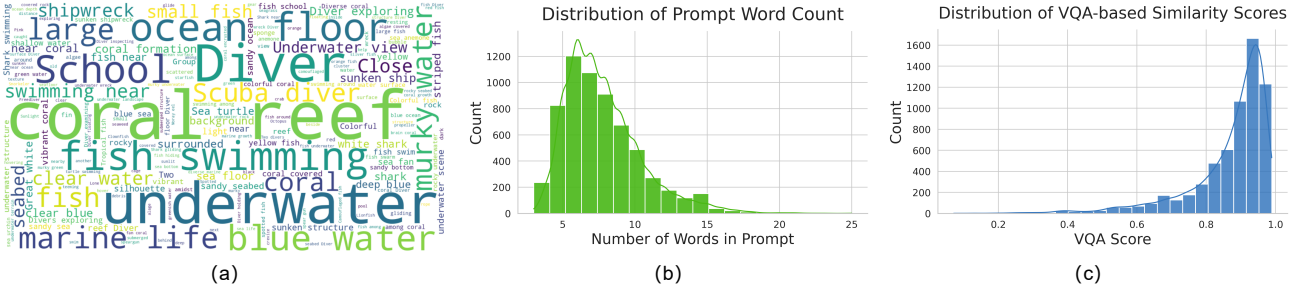


Fig. 3. Statistical analysis of the LUQID-TD textual annotations, including (a) word-frequency patterns, (b) the distribution of caption lengths, and (c) the distribution of VQA-based image–text consistency scores, demonstrating the semantic quality and reliability of the annotations.

To ensure accuracy and semantic consistency, the textual descriptions were initially generated using ChatGPT-4². We then individually reviewed and refined all captions, making necessary adjustments to guarantee that the descriptions faithfully capture the scene content, maintain consistent terminology, and avoid semantic ambiguity. This hybrid caption pipeline combines the scalability of automatic generation with the reliability of manual refinement, ensuring both efficiency and annotation quality. As a result, we obtain 6,418 multimodal triplets in the form:

$$\mathcal{D}_i = (\mathbf{I}_i^{raw}, \mathbf{I}_i^{ref}, T_i), \quad i = 1, \dots, 6418. \quad (1)$$

This triplet design enables text-conditioned underwater image enhancement, where models improve degraded inputs not only based on visual information but also guided by semantic cues. Representative examples are shown in Fig. 2. In addition, Fig. 3 provides a statistical overview of the textual annotations, including word-frequency distribution, caption length distribution, and image–text similarity scores, further

demonstrating the semantic quality and consistency of the LUQID-TD descriptions.

To the best of our knowledge, LUQID-TD is the first large-scale vision–language data set dedicated to underwater image enhancement. By providing aligned raw-reference pairs and high-quality textual annotations, LUQID-TD bridges the gap between low-level restoration and high-level semantics. It offers a novel benchmark for text-guided enhancement, multimodal supervision, and semantic evaluation, fostering the development of next-generation multimodal UIE methods.

IV. METHODOLOGY

Motivated by the Retinex theory [5], we propose the Physics- and Semantics-Guided Underwater Image Enhancement Network (PSG-UIENet). As shown in Fig. 4, this network is designed to integrate physical priors with high-level semantic guidance, enabling more perceptually meaningful underwater image enhancement. PSG-UIENet comprises two main components: a prior-free illumination estimator and a semantics-guided image restorer. Compared with existing approaches, PSG-UIENet effectively utilizes both physical

²<https://chatgpt.com/>

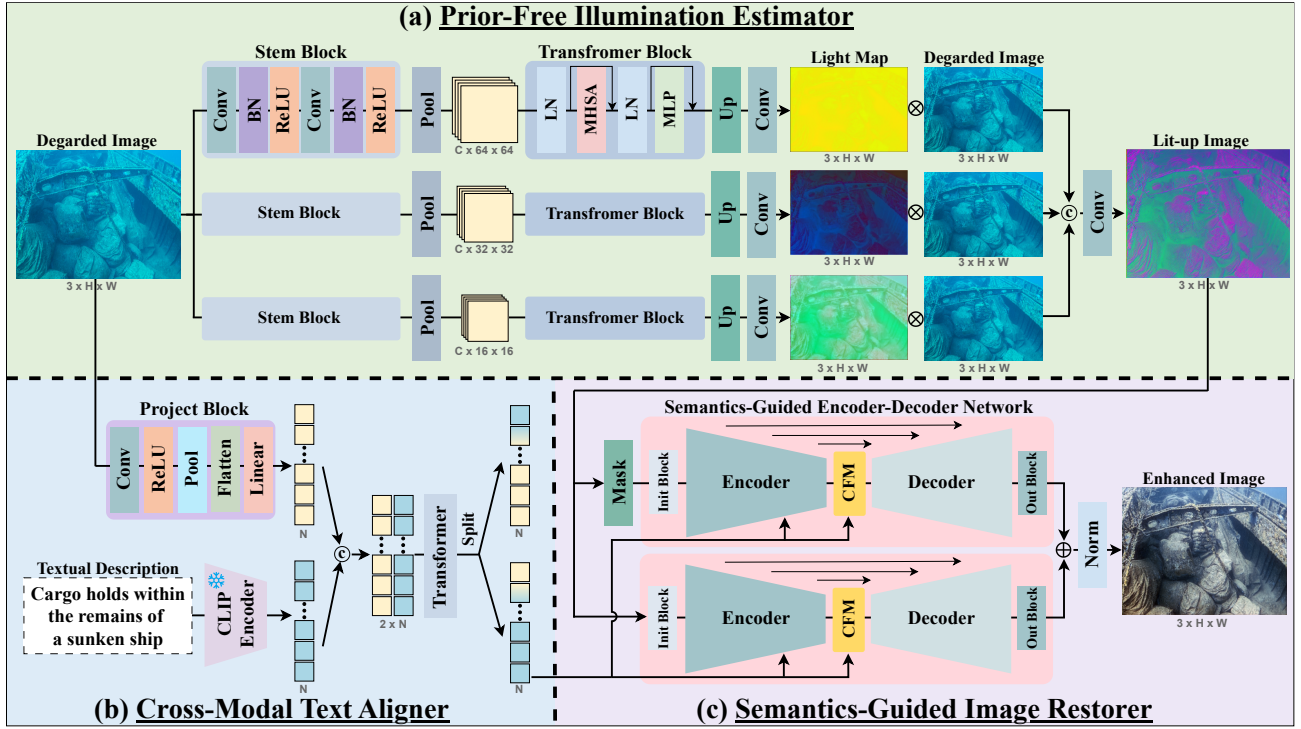


Fig. 4. The overall architecture of the proposed PSG-UIENet, which comprises three modules: (a) a Prior-Free Illumination Estimator that generates multi-scale light-enhanced representations, (b) a Cross-Modal Text Aligner that establishes semantic correspondence between text and image, and (c) a Semantics-Guided Image Restorer that performs multimodal fusion and enhancement using a dual-branch structure.

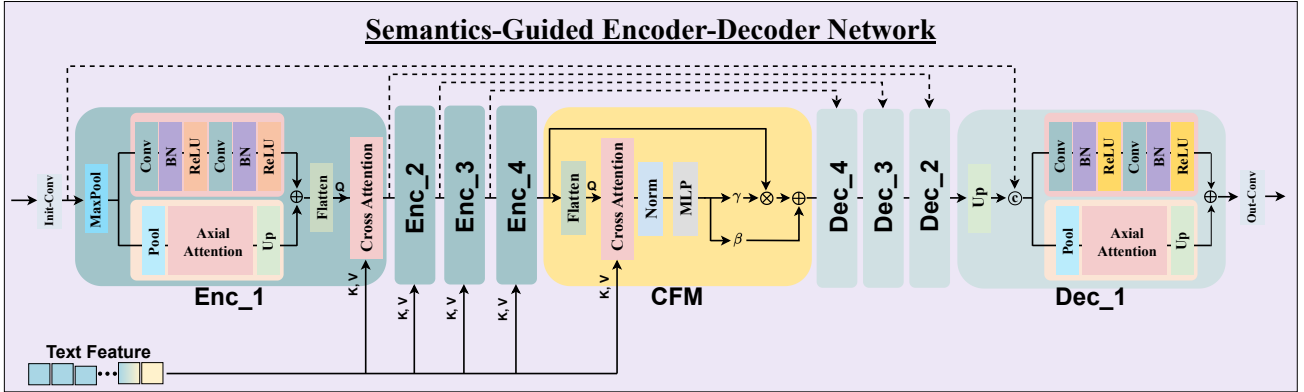


Fig. 5. Architecture of the Semantics-Guided Encoder-Decoder Network. The symmetric encoder–decoder uses Transformer-Conv modules for joint local-global feature extraction. Cross-modal attention and a Cross-Attention FiLM Module (CFM) integrate textual semantics, enabling progressive image reconstruction with semantic and visual fusion.

theory and semantic guidance, achieving superior performance in complex real-world underwater scenarios.

A. Motivation

The Retinex theory, first proposed by Land [21], models the Human Visual System (HVS) by decomposing an image into two components: reflectance, representing the intrinsic properties of the scene, and illumination, influenced by environmental lighting. This decomposition is expressed as:

$$I(x) = R(x) \cdot L(x), \quad (2)$$

where $R(x)$ denotes the reflectance, and $L(x)$ represents the illumination. Retinex theory has inspired numerous image

enhancement methods due to its strong physical interpretability. Although effective in many scenarios, the vanilla formulation faces significant challenges in underwater environments. The unique optical properties of water, such as nonuniform lighting, severe color cast, scattering, backscatter, and sensor noise, make direct estimation of $R(x)$ and $L(x)$ highly brittle. To address these limitations, recent works have extended Retinex theory with perturbation-aware formulations [17], [18], introducing perturbation terms to account for deviations in reflectance and illumination. Building on these insights, we reformulate the Retinex decomposition to better handle underwater complexities. Specifically, we introduce perturbation terms \hat{R} and \hat{L} to model deviations from ideal reflectance and

illumination:

$$\begin{aligned} I_{raw} &= (R + \hat{R}) \odot (L + \hat{L}) \\ &= R \odot L + R \odot \hat{L} + \hat{R} \odot (L + \hat{L}), \end{aligned} \quad (3)$$

where $\hat{R} \in \mathbb{R}^{H \times W \times 3}$ and $\hat{L} \in \mathbb{R}^{H \times W}$ represent perturbation terms for reflectance and illumination, respectively.

To simplify the computation and mitigate illumination imbalance, we further apply an element-wise multiplication on both sides of Eq. (3) with a normalized light map \bar{L} , where $\bar{L} \odot L = 1$. resulting in:

$$\begin{aligned} I_{raw} \odot \bar{L} &= (R \odot L + R \odot \hat{L} + \hat{R} \odot (L + \hat{L})) \odot \bar{L} \\ &= R + R \odot (\hat{L} \odot \bar{L}) + (\hat{R} \odot (L + \hat{L})) \odot \bar{L}. \end{aligned} \quad (4)$$

After simplification, the illuminated image I_{lit} can be expressed as:

$$I_{lit} = I_{raw} \odot \bar{L} = R + C, \quad (5)$$

where $I_{lit} \in \mathbb{R}^{3 \times H \times W}$ is the light-enhanced image, $R \in \mathbb{R}^{3 \times H \times W}$ corresponds to the ideally exposed image (i.e., the final enhanced image I_{enh}), and $C \in \mathbb{R}^{3 \times H \times W}$ is the residual perturbation term.

This decomposition motivates a two-stage solution for underwater image enhancement. First, we estimate \bar{L} in a data-driven, prior-free manner to obtain I_{lit} . This step mitigates exposure and illumination imbalances, producing a well-normalized image. Second, we reduce the residual perturbation term C by restoring contrast, color fidelity, and fine details. This process is guided by high-level semantic features extracted from textual descriptions.

As shown in Fig. 4, the Illumination Estimator explicitly models multi-scale illumination maps and generates an initially light-enhanced image through an adaptive fusion mechanism. To incorporate semantic information into the enhancement process, the Image Restorer leverages the semantic understanding capability of the CLIP model [22] and introduces a novel Semantics-Guided Restorer. This module consists of three parallel branches: two of them employ complementary masking strategies to selectively fuse image and text features, while the third branch processes the unmasked original image features to preserve global consistency and fine details.

B. PSG-UIENet

As illustrated in Fig. 4, the proposed Physics- and Semantics-Guided Underwater Image Enhancement Network (PSG-UIENet) is designed to jointly leverage physical priors and high-level semantics for perceptually meaningful underwater image enhancement. The architecture is composed of two main components: (i) a Prior-Free Illumination Estimator that captures multi-scale illumination characteristics without relying on handcrafted priors, and (ii) a Semantics-Guided Image Restorer that exploits textual guidance to refine visual details through dual-branch cross-modal fusion. The end-to-end enhancement pipeline is summarized in Algorithm 1.

Algorithm 1 Process of PSG-UIENet Model

Input: Raw underwater image I_{raw} , text description T

Output: Enhanced image I_{enh}

- 1: // **Prior-Free Multi-Scale Illumination Estimation**
 - 2: **for** each scale s in $\{16, 32, 64\}$ **do**
 - 3: Estimate illumination maps \bar{L}_s from I_{raw} ;
 - 4: Compute lit-up image $I_{lit_s} = I_{raw} \odot \bar{L}_s$;
 - 5: **end for**
 - 6: Fuse $\{I_{lit_{16}}, I_{lit_{32}}, I_{lit_{64}}\}$ to obtain final lit-up image I_{lit} ;
 - 7: // **Cross-Modal Text Aligner**
 - 8: Flatten I_{raw} into 1D feature vector F_{img} ;
 - 9: Encode text T_{TD} via frozen CLIP text encoder to get F_{text} ;
 - 10: Concatenate F_{img} and F_{text} into joint feature F_{joint} ;
 - 11: Feed F_{joint} into Transformer to obtain aligned features $[F'_{img}, F'_{text}]$;
 - 12: Extract text-aligned feature F'_{text} for guidance;
 - 13: // **Semantics-Guided Image Restoration**
 - 14: Generate mask M_θ from I_{raw} ;
 - 15: // *Semantics Branch:*
 - 16: Compute $I_1 = I_{raw} \odot M_\theta$;
 - 17: Pass I_1 through semantics-guided encoder-decoder network, using F'_{text} ;
 - 18: Get intermediate output \hat{I}_1 ;
 - 19: // *Image Branch:*
 - 20: Pass I_{raw} through another identical semantics-guided encoder-decoder network, using F'_{text} ;
 - 21: Get intermediate output \hat{I}_2 ;
 - 22: // **Output**
 - 23: Compute fused output: $\hat{I} = \text{Norm}(\hat{I}_1 + \hat{I}_2)$;
 - 24: **return** \hat{I}
-

coupling domain-agnostic physical enhancement with contextual semantics, PSG-UIENet simultaneously addresses low-level photometric distortions and high-level perceptual fidelity in challenging underwater environments.

1) *Prior-Free Illumination Estimator:* As shown in Fig. 4(a), the Prior-Free Illumination Estimator computes multi-scale illumination maps in a data-driven manner without relying on explicit physical priors. It utilizes adaptive average pooling to capture diverse lighting degradations across three spatial resolutions: 16×16 , 32×32 , and 64×64 . At each scale s , an Illumination Estimation Module (IE_s) predicts the illumination map \bar{L}_s :

$$\bar{L}_s = IE_s(I_{raw}), \quad s = 16, 32, 64. \quad (6)$$

Each IE_s consists of a Stem block and Transformer Block, which are responsible for encoding both local and global illumination contexts. To compute the scale-specific lit-up images, the model applies an element-wise multiplication with the input image:

$$I_{lit_s} = I_{raw} \odot \bar{L}_s. \quad (7)$$

The lit-up images from all scales are then fused using an adaptive convolutional fusion strategy:

$$I_{lit} = \text{Conv}(\text{Concat}(I_{lit_{16}}, I_{lit_{32}}, I_{lit_{64}})). \quad (8)$$

This hierarchical estimation and fusion mechanism enables the model to robustly handle diverse lighting degradations in underwater scenarios and provides a well-normalized input for subsequent semantics-guided restoration.

2) *Semantics-Guided Image Restorer*: To address the challenges of underwater image restoration, we propose a novel semantics-guided image restoration framework that integrates high-level textual semantics into the enhancement process. As illustrated in Fig. 4(c), the framework incorporates a dual-branch architecture guided by textual semantics and enhanced through a masking-based learning strategy.

Inspired by the semantic learning mechanism in Masked Autoencoders (MAE) [35], we apply a pixel-wise random binary mask M_θ with a predefined masking ratio θ to the illumination-enhanced image I_{lit} . The masking process generates two inputs for the dual-branch network:

$$I_1 = I_{lit} \odot M_\theta, \quad I_2 = I_{lit}. \quad (9)$$

Here, I_1 serves as the input to the semantics branch, which focuses on reconstructing occluded regions by attending to textual semantics. The masked input compels the network to rely on contextual clues and semantic priors extracted from the text, thereby reinforcing high-level understanding of the visual content. In contrast, the unmasked input I_2 drives an image branch, which operates on the complete illumination-enhanced image to preserve structural integrity and enhance fine-grained visual details.

To unify the processing of both branches, we design a semantics-guided encoder–decoder network (SGED) that integrates visual and textual modalities through cross-modal fusion mechanisms. The outputs of the semantics branch and the image branch are denoted as \hat{I}_1 and \hat{I}_2 , respectively:

$$\hat{I}_i = \text{SGED}(I_i), \quad i = 1, 2. \quad (10)$$

Finally, the outputs from both branches are aggregated using an additive fusion strategy, followed by normalization to produce the final enhanced image:

$$I_{enh} = \text{Norm}(\hat{I}_1 + \hat{I}_2). \quad (11)$$

The overall architecture is designed in an encoder–decoder style with a bottleneck structure. Each encoder adopts a Transformer–Conv module for mixed long-range and local feature extraction, followed by a Fuse block that injects text features via cross-modal attention. At the bottleneck layer, we introduce a Cross-Attention FiLM Module (CFM), which utilizes global text feature extracted by CLIP to generate channel-wise scaling and shifting parameters. These parameters are used to dynamically modulate the visual feature maps, further improving semantic alignment and contextual adaptability. The decoder employs residual connections to combine shallow visual details with deep fused semantics, and progressively reconstructs the image via stacked Transformer–Conv modules, yielding outputs that are both structurally faithful and semantically coherent.

Cross-Modal Text Aligner. As illustrated in Fig. 4(b), the Cross-Modal Text Aligner module establishes precise semantic

correspondence between image features and textual representations, serving as a key component for enabling multimodal collaborative enhancement. While CLIP [22] provides a generic cross-modal alignment capability, its training data includes limited underwater imagery, leading to potential semantic bias. To mitigate this problem, we introduce a learnable projection block $PB(\cdot)$ to map raw image features into a unified semantic embedding space:

$$E_{img} = PB(I_{raw}), \quad E_{text} = \phi(T_{TD}), \quad (12)$$

where $\phi(\cdot)$ represents the frozen CLIP text encoder producing global text embeddings from the input description T_{TD} . To enable deep interaction between these cross-modal embeddings, we employ a Transformer encoder equipped with multi-head attention mechanisms. Specifically, the image and text embeddings are concatenated and processed as follows:

$$\begin{aligned} (E'_{img}, F'_{text}) &= CMTA(E_{img}, E_{text}) \\ &= T_{MHA}(\text{Concat}(E_{img}, E_{text})), \end{aligned} \quad (13)$$

where $CMTA(\cdot)$ denotes the cross-modal text aligner module, and $T_{MHA}(\cdot)$ refers to the Transformer encoder equipped with multi-head attention mechanisms. As a critical bridging component in the overall architecture, the cross-modal text aligner module provides a precise alignment foundation for subsequent semantics-guided enhancement, thereby significantly improving the semantic consistency and perceptual quality of the enhanced results.

Semantics-Guided Encoder-Decoder Network. As illustrated in Fig. 5, the Semantics-Guided Encoder-Decoder Network (SGED) is designed to deeply integrate visual and textual modalities for underwater image restoration. It follows an encoder–bottleneck–decoder architecture, where the encoder extracts hierarchical visual features, the bottleneck dynamically fuses visual and textual information, and the decoder progressively reconstructs the enhanced image. The core innovation lies in the bottleneck layer, where we introduce the *Cross-Attention FiLM Module (CFM)* to achieve fine-grained semantic integration and adaptive feature modulation.

The encoder processes the input image through a sequence of Transformer-Conv layers, which are designed to capture both local and global features:

$$\begin{aligned} F'_{img} &= TC(F_{img}) \\ &= T_{AST}(F_{img}) + \text{Conv}_D(F_{img}), \end{aligned} \quad (14)$$

where $\text{Conv}_D(\cdot)$ consists of two consecutive 3×3 convolutional layers, each followed by Batch Normalization and ReLU activation, and $T_{AST}(\cdot)$ denotes the axial self-attention mechanism [15]. This combination ensures efficient extraction of both spatial details and global contextual information, which are essential for handling the complex degradations in underwater images. The encoded image features F'_{img} are then fused with the aligned text features F'_{text} , obtained from the Cross-Modal Text Aligner, through a cross-modal Fuse module based on multi-head cross-attention:

$$\begin{aligned} F_{fuse} &= \text{Fuse}(F'_{img}, F'_{text}) \\ &= \text{LayerNorm}(CA(F'_{img}, F'_{text}) + F'_{img}), \end{aligned} \quad (15)$$

where $CA(\cdot)$ denotes the multi-head cross-attention operation, which leverages image features as queries and text features as keys and values to inject semantic information into the visual representation. The fused representation is passed through a residual connection followed by layer normalization to preserve original visual context while injecting semantic information.

The decoder mirrors the encoder with stacked Transformer–Conv blocks, and employs residual connections to merge shallow visual details with deep semantic features. This progressive reconstruction yields outputs that are both structural fidelity and semantic coherence, enabling high-quality, perceptually aligned enhancement results.

Cross-Attention FiLM Module. At the bottleneck of SGED, to facilitate more effective cross-modal semantic integration during image restoration, we propose the Cross-Attention FiLM Module (CFM) as an extension to the conventional Feature-wise Linear Modulation (FiLM) [36] framework. While the traditional FiLM mechanism generates channel-wise scaling (γ) and shifting (β) parameters directly from class labels or static textual embeddings, it lacks the capacity to explicitly model the interaction between visual content and corresponding textual semantics, thereby limiting its applicability in multimodal scenarios. To address this limitation, CFM augments FiLM with a cross-attention stage that aligns visual features with global textual cues before producing modulation parameters. Specifically, image features act as queries and text features as keys or values in a multi-head cross-attention block. The resulting fused representation encodes the relevance between visual regions and semantic tokens, which is then aggregated via global average pooling (GAP) and passed through a multi-layer multilayer perceptron (MLP) to generate modulation parameters:

$$(\gamma, \beta) = MLP(GAP(CA(F_{img}, F'_{text}))). \quad (16)$$

The resulting γ and β vectors are reshaped and applied to the original image features through channel-wise affine transformation:

$$F'_{fuse} = F_{img} \odot \gamma + \beta. \quad (17)$$

where \odot denotes element-wise multiplication along the channel dimension. In contrast to the original FiLM [36], which statically conditions the modulation on fixed embeddings, the proposed CFM dynamically infers modulation parameters from rich cross-modal interactions. This allows semantic information to be injected into the restoration process in a more adaptive and fine-grained manner, ultimately improving both the semantic coherence and perceptual fidelity of the enhanced underwater images.

C. Loss Functions

To achieve high-quality underwater image restoration, we design a composite loss function that balances pixel-level fidelity, structural consistency, perceptual realism, and semantic alignment. The loss function integrates four components: MSE loss, SSIM loss, perceptual loss, and an image-text semantic similarity loss.

1) *Image-Text Semantic Similarity Loss.*: To explicitly incorporate high-level semantic guidance, we propose a novel image-text semantic similarity loss (ITSS). Unlike traditional losses that rely solely on visual references, \mathcal{L}_{ITSS} ensures that the enhanced image aligns semantically with a corresponding textual description T , while maintaining consistency with the raw input I_{raw} . This is particularly critical for underwater scenes, where semantic cues are often degraded or obscured. We leverage a pretrained CLIP model [22] to encode image and text embeddings into a shared latent space. Let $\phi(\cdot)$ denote the CLIP encoder, and $\cos(\cdot, \cdot)$ represent the cosine similarity function. The loss is formulated as:

$$\mathcal{L}_{ITSS} = |\cos(\phi(I_{enh}), \phi(T)) - \cos(\phi(I_{ref}), \phi(T))|, \quad (18)$$

This formulation introduces cross-modal supervision and serves as a semantic anchor that aligns the enhancement process with human intent. It is particularly beneficial for underwater scenes, where semantic cues are often lost due to severe degradation. By embedding high-level textual guidance into the optimization process, \mathcal{L}_{ITSS} acts as a semantic anchor, enabling the model to produce enhancements that are both visually plausible and semantically meaningful.

2) *Total Loss.*: The final loss function used to train the network is a weighted combination of all components:

$$\mathcal{L}_{total} = \mathcal{L}_{MSE} + \mathcal{L}_{SSIM} + \alpha \cdot \mathcal{L}_{Perceptual} + \beta \cdot \mathcal{L}_{ITSS}. \quad (19)$$

where α and β are hyperparameters to balance the contribution of perceptual and semantic alignment terms.

Here, \mathcal{L}_{MSE} ensures pixel-wise accuracy, while \mathcal{L}_{SSIM} emphasizes structural consistency. To further improve perceptual quality, $\mathcal{L}_{Perceptual}$ compares high-level features extracted from a pretrained VGG network. Finally, \mathcal{L}_{ITSS} is specifically designed to enforce text–image semantic consistency, serving as a unique component tailored for multimodal underwater enhancement.

V. EXPERIMENTAL SETTINGS

In this section, we will briefly introduce the baselines, data sets, evaluation metrics and implementation details utilized in our experiments.

A. Baselines

We compared the proposed method with six prior-based approaches, including UDCP [2], Retinex [5], HE [37], HLRP [6] and MMLE [7] and HFM [8]. We also compared our method with four learning-based approaches which did not consider the Retinex theory [5], including PUIE-Net [12], U-Transformer [13], UWFormer [16] and PATS-UIENet [11], three learning-based approaches which were developed on top of the Retinex theory [5], including Retinexformer [17], CCMSRNet [15] and RetinexMamba [18], and two text-guided multimodal approaches, including CLIP-LIT [23] and CLIP-UIE [25].

B. Data Sets

We conducted a series of experiments on four publicly available real-world underwater image data sets, namely *LUIQD-TD*, *UIEB* [9], *SUIM-E* [33], and *SQUID* [4]. The proposed *LUIQD-TD* data set in Sec.III contains a total of 6,418 image pairs, where each reference image is selected from the results of nine enhancement algorithms applied to a degraded image. Due to 194 duplicate degraded images in the data set, these pairs were removed, resulting in a final set of 6,224 image pairs used for experiments.

Similarly, the *UIEB* data set originally includes 890 image pairs, with each reference image manually selected from the results of 12 enhancement algorithms. Ten pairs were removed due to duplicated degraded images, leaving 880 pairs in total. The *SUIM-E* [33] data set consists of 1,525 degraded image pairs and a test set of 110 labeled images. The *SQUID* [4] data set, captured using a stereo camera, includes 114 underwater images.

We randomly split the *LUIQD-TD* data set into training, validation, and testing sets in a ratio of 8:1:1. The testing set, consisting of 622 image pairs, is used as the first test set and is referred to as Test-L622. In the *UIEB* [9] data set, 80 image pairs were randomly selected as the second test set, named Test-U80. An additional 60 challenging images without reference images were included as the third test set, named Test-C60. The fourth test set, Test-S110, consists of 110 labeled image pairs from the *SUIM-E* [33] data set. Finally, 53 images captured by the right-hand camera from the *SQUID* [4] data set were randomly selected and used as the fifth test set, referred to as Test-R53.

C. Evaluation Metrics

For test data with reference images, we employed Peak Signal-to-Noise Ratio (PSNR), Structural Similarity Index (SSIM) [19], and Learned Perceptual Image Patch Similarity (LPIPS) [20] to evaluate the quality differences between the enhanced images and their corresponding references. For test data without reference images, considering that traditional metrics such as Underwater Color Image Quality Evaluation (UCIQE) [38] and Underwater Image Quality Measure (UIQM) [39] have been reported in multiple studies [14], [26], [33] to exhibit significant inconsistencies with human visual perception, we adopted the Perception-Aware Underwater Image Quality Assessment (PAUQA) [26] and the Underwater Image Fidelity (UIF) [40] as the primary no-reference quality assessment methods.

D. Implementation Details

We implemented PSG-UIENet using the PyTorch framework and conducted all experiments on a machine equipped with an NVIDIA RTX 3090 GPU and Ubuntu 20.04 operating system. During training, all input and reference images were resized to a spatial resolution of 256×256 . We trained PSG-UIENet on the training set of the proposed *LUIQD-TD* data set. Model training was conducted using distributed data parallelism (DDP) to accelerate convergence, and automatic mixed precision (AMP) was enabled for computational

efficiency. The network was optimized using the AdamW optimizer, with an initial learning rate of 1×10^{-4} and a batch size of 4. The total number of training epochs was set to 100. The CLIP model used in our method is ViT-B/32, with frozen weights during training. During semantic-guided image restoration, we adopt a pixel-wise random masking strategy with a fixed masking ratio of $\theta = 0.5$. And the hyperparameters of loss functions, α and β , were empirically set to 0.1 and 0.0001, respectively. Notably, for test images lacking textual descriptions, we used a unified default prompt “An underwater image” as the input to the CLIP text encoder to maintain consistency across the testing pipeline.

VI. EXPERIMENTAL RESULTS

In this section, we will report the results obtained in the underwater image enhancement, and the ablation study.

A. Full-Reference Quantitative Evaluation

Since the Test-L622, Test-U80, and Test-S110 data sets all contain reference images, we conducted full-reference quantitative evaluations on the proposed method and 15 representative baselines using Peak Signal-to-Noise Ratio (PSNR), Structural Similarity Index (SSIM) [19], and Learned Perceptual Image Patch Similarity (LPIPS) [20]. The evaluation results are summarized in Table I. As observed, our PSG-UIENet generally achieves the best performance across all three metrics on each testing set. Compared with Retinex-based methods (e.g., Retinex [5], Retinexformer [17], CCM-SRNet [15], and RetinexMamba [18]) and existing text-guided cross-modal approaches (e.g., CLIP-LIT [23] and CLIP-UIE [25]), our method consistently demonstrates more significant advantages.

B. Non-reference Quantitative Evaluation

We employed two no-reference image quality assessment metrics, PAUQA [26] and UIF [40], to evaluate the performance of our proposed method and 15 baseline methods on five testing sets: Test-L622, Test-U80, Test-S110, Test-C60, and Test-R53. The results are presented in Table II. As shown, our method generally achieved second-best performance across these data sets.

Specifically, in terms of the PAUQA metric, CCM-SRNet [15] obtained the highest scores on all five testing sets, while our method consistently ranked second across all of them. Regarding the UIF metric, CLIP-LIT [23] achieved the best performance across the five data sets. Although our method did not always secure the second-best scores in UIF, it still demonstrated competitive performance on several challenging testing sets, such as Test-L622, Test-U80, and Test-S110.

C. Qualitative Analysis

The enhanced images generated by our method and 15 baseline approaches on five testing sets are shown in Figs. 6 to Figs. 10. It can be observed that some methods achieving higher scores in LPIPS [20], PAUQA [26], and UIF [40] metrics did not yield visually satisfactory results. For instance,

TABLE I

THE FULL-REFERENCE QUANTITATIVE EVALUATION OF THE PROPOSED PSG-UIENET AND FIFTEEN BASELINES ON THREE REAL-WORLD TESTING SETS. THE BEST AND SECOND BEST RESULTS ARE HIGHLIGHTED IN THE **RED BOLD** AND *Blue Italic* FONTS, RESPECTIVELY.

Method	Test-T622			Test-U80			Test-S110		
	PSNR \uparrow	SSIM \uparrow	LPIPS \downarrow	PSNR \uparrow	SSIM \uparrow	LPIPS \downarrow	PSNR \uparrow	SSIM \uparrow	LPIPS \downarrow
UDCP [2]	11.51	47.60	26.94	9.51	33.66	41.74	10.07	34.29	37.66
Retinex [5]	10.56	58.10	39.12	10.50	61.31	36.49	8.32	53.46	40.41
HE [37]	16.01	71.30	28.07	16.60	77.86	25.67	15.41	74.79	30.05
HLRP [6]	13.00	23.83	33.11	13.56	22.76	33.90	12.55	29.24	33.18
MMLE [7]	17.07	72.11	25.41	18.56	76.21	22.57	17.32	77.39	22.77
HFM [8]	16.92	77.73	25.18	18.35	83.01	19.70	15.62	77.28	26.06
PUIE-Net [12]	23.01	89.03	10.20	20.45	87.23	15.29	21.71	89.89	9.47
U-Transformer [13]	19.97	57.70	44.82	20.82	72.42	30.20	20.34	68.74	31.07
UWFormer [16]	22.65	87.69	9.92	19.17	83.82	17.79	<i>22.69</i>	<i>91.48</i>	<i>8.29</i>
PATS-UIENet [11]	22.95	88.42	10.39	21.64	<i>88.92</i>	<i>12.62</i>	22.68	91.03	8.58
Retinexformer [17]	23.24	90.06	9.02	20.71	87.83	14.19	22.27	90.99	8.67
CCMSRNet [15]	23.10	88.55	11.31	<i>21.83</i>	88.42	13.62	22.36	90.14	9.63
RetinexMamba [18]	<i>23.42</i>	<i>90.09</i>	<i>9.08</i>	20.20	87.36	14.97	22.47	91.26	8.55
CLIP-LIT [23]	13.39	70.51	25.04	11.17	64.42	42.00	13.65	76.71	23.10
CLIP-UIE [25]	18.63	67.05	35.97	18.51	74.86	30.94	18.66	75.55	26.63
PSG-UIENet (Ours)	24.07	90.19	9.11	23.01	90.76	10.49	23.60	92.37	7.41

TABLE II

THE NON-REFERENCE QUANTITATIVE EVALUATION OF THE PROPOSED PSG-UIENET AND FIFTEEN BASELINES ON FIVE REAL-WORLD TESTING SETS. THE BEST AND SECOND BEST RESULTS ARE HIGHLIGHTED IN THE **RED BOLD** AND *Blue Italic* FONTS, RESPECTIVELY.

Method	Test-L622		Test-U80		Test-S110		Test-C60		Test-R53	
	PAUQA \uparrow	UIF \uparrow								
UDCP [2]	36.71	55.91	29.73	36.40	29.92	32.01	28.19	25.41	33.07	3.24
Retinex [5]	36.83	46.41	34.38	49.83	31.79	39.43	29.20	49.85	37.52	2.61
HE [37]	41.32	45.10	37.82	44.04	34.26	45.01	34.69	41.50	34.95	1.67
HLRP [6]	36.83	0.57	38.12	0.59	37.33	0.91	30.16	3.57	28.53	1.26
MMLE [7]	45.26	37.88	43.49	30.99	43.15	35.05	37.06	24.95	33.15	24.67
HFM [8]	42.78	50.13	42.24	55.31	37.55	44.46	36.76	49.80	32.45	31.50
PUIE-Net [12]	49.78	62.60	45.42	<i>63.91</i>	49.15	59.80	41.45	<i>52.76</i>	41.23	<i>43.56</i>
U-Transformer [13]	45.82	24.56	45.26	39.43	45.97	25.33	41.47	30.52	40.51	19.25
UWFormer [16]	48.44	53.23	42.41	47.98	48.64	56.10	38.70	37.39	40.31	36.27
PATS-UIENet [11]	49.99	67.66	45.58	58.63	48.64	62.53	41.11	47.77	39.02	43.51
Retinexformer [17]	51.02	66.94	45.43	61.63	49.34	60.05	41.45	60.49	40.90	37.70
CCMSRNet [15]	52.04	60.91	47.66	53.51	51.74	55.83	42.86	43.79	42.25	34.39
RetinexMamba [18]	50.91	66.20	45.09	61.44	49.03	58.40	41.34	39.47	40.48	35.42
CLIP-LIT [23]	46.76	70.89	37.92	70.93	45.71	66.64	37.44	54.65	36.81	57.50
CLIP-UIE [25]	45.79	61.00	41.33	54.87	44.72	53.98	37.93	41.12	36.94	30.24
PSG-UIENet (Ours)	<i>51.34</i>	<i>67.70</i>	<i>46.32</i>	59.46	<i>49.37</i>	<i>62.60</i>	<i>41.63</i>	49.87	<i>41.32</i>	42.65

although Retinexformer [17] and RetinexMamba [18] achieved the highest and second-highest LPIPS [20] scores on Test-U80, their results exhibited noticeable color distortion (see Fig. 7). In contrast, our PSG-UIENet effectively improved various types of degraded images and produced enhanced results with natural and vivid colors. Similarly, although CLIP-LIT [23] achieved the highest UIF [40] scores across all five testing sets, its visual results, as shown in Figs. 6 to 10, were not consistently satisfactory. While our method may yield slightly lower PAUQA [26] or UIF [40] scores compared to some baselines, like [12], [15], [23], the enhanced images still demonstrate superior subjective visual quality.

D. Ablation Study

To evaluate the effectiveness of each component in the proposed PSG-UIENet, we conducted a series of ablation

experiments on the Test-L622 data set. These experiments were designed to isolate and analyze the contributions of individual modules, the text modality, the masking strategy, and the loss hyperparameters. The evaluation was carried out using both full-reference metrics, PSNR, SSIM and LPIPS, and a no-reference quality metric, PAUQA.

1) *Effect of the Components of PSG-UIENet*: To investigate the contribution of each core component in PSG-UIENet, we conducted an ablation study by individually removing the Illumination Estimator (w/o IE), Image Restorer (w/o IR), Text Aligner (w/o TA), and Cross-Attention FiLM Module (w/o CFM). As shown in Table III, removing any component results in a performance decline across one or more metrics, confirming their individual effectiveness. Removing the Image Restorer (IR) causes the most significant drop in PSNR and SSIM, indicating its essential role in structural reconstruction.

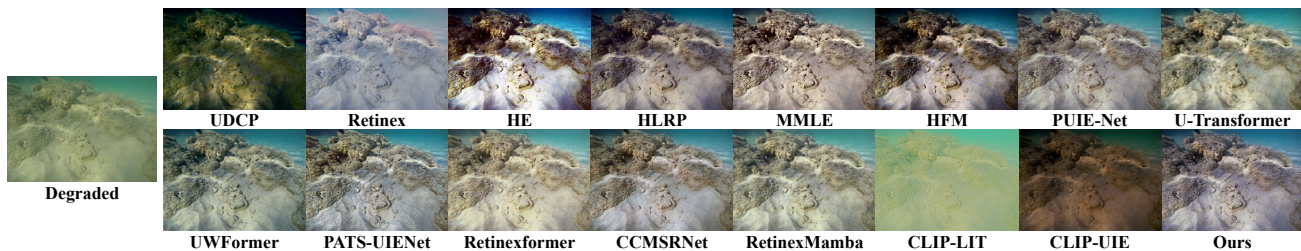


Fig. 6. The results produced by 15 baselines and our method in terms of a degraded image in the Test-L622 testing set.

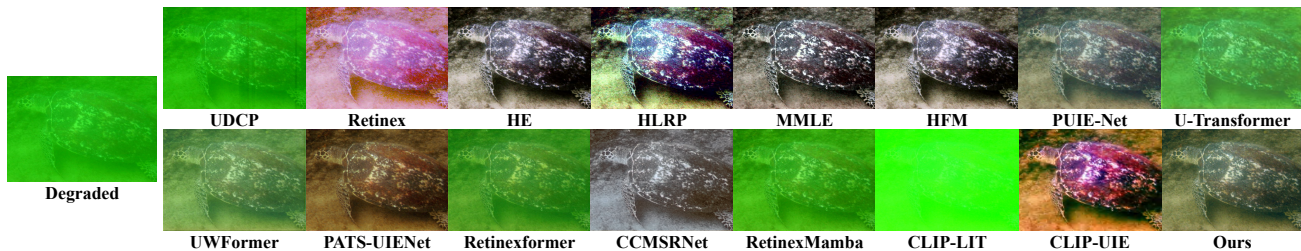


Fig. 7. The results produced by 15 baselines and our method in terms of a degraded image in the Test-U80 testing set.

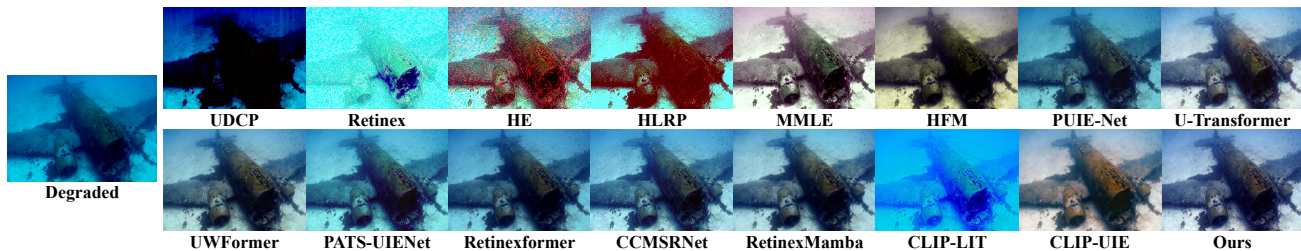


Fig. 8. The results produced by 15 baselines and our method in terms of a degraded image in the Test-S110 testing set.

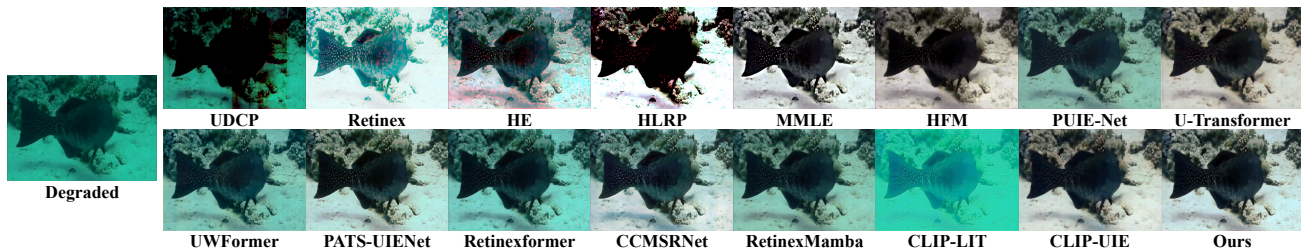


Fig. 9. The results produced by 15 baselines and our method in terms of a degraded image in the Test-C60 testing set.

The removal of the Text Aligner (TA) achieves the lowest LPIPS, but slightly reduces PAUQA and PSNR, suggesting it enhances perceptual detail at the cost of semantic or structural balance. In contrast, excluding the CFM slightly degrades PAUQA and LPIPS, underscoring its importance in semantic modulation. Overall, the full PSG-UIENet configuration achieves the best balance across all metrics.

2) *Effect of the Text Modality*: To evaluate the role of textual guidance in our framework, we compared the full model with two variants: one that entirely removes the text modality (w/o Text), and another that replaces our proposed cross-attention mechanism with standard multi-head self-attention (w/ MHA). As shown in Table IV, removing the text stream leads to a noticeable performance drop in PSNR, SSIM, and LPIPS, despite slightly higher PAUQA. This suggests that although the overall perceptual quality may remain stable,

TABLE III
COMPARISON BETWEEN OUR METHOD AND ITS FOUR VARIANTS OBTAINED BY REMOVING ONE OF THE KEY COMPONENTS IN PSG-UIENET.

Variant	Test-L622			
	PSNR \uparrow	SSIM \uparrow	LPIPS \downarrow	PAUQA \uparrow
w/o IE	23.49	89.70	9.56	51.27
w/o IR	22.44	86.47	11.60	48.73
w/o TA	23.69	90.11	8.90	51.10
w/o CFM	23.62	89.73	9.21	50.78
Ours	24.07	90.19	9.11	51.34

structural and semantic fidelity are compromised. In addition, replacing the cross-attention mechanism with conventional multi-head self-attention also leads to performance degradation across all metrics, further validating the effectiveness of our

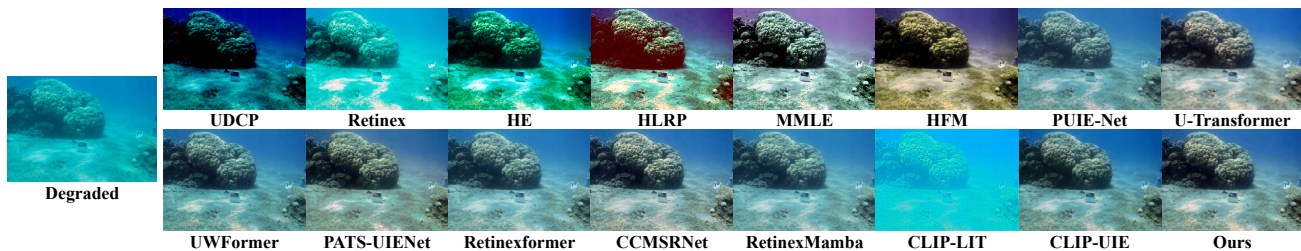


Fig. 10. The results produced by 15 baselines and our method in terms of a degraded image in the Test-R53 testing set.

TABLE IV

COMPARISON BETWEEN OUR METHOD AND ITS TWO VARIANTS OBTAINED BY REMOVING THE TEXT MODALITY OR REPLACING THE CROSS-ATTENTION MECHANISM WITH MHA.

Variant	Test-L622			
	PSNR \uparrow	SSIM \uparrow	LPIPS \downarrow	PAUQA \uparrow
w/o Text	23.66	89.93	9.21	51.48
w/ MHA	23.25	89.52	9.61	51.03
Ours	24.07	90.19	9.11	51.34

TABLE V

COMPARISON BETWEEN OUR METHOD AND ITS FOUR VARIANTS OBTAINED BY CHANGING THE MASK RATIO θ .

Mask Ratio θ	Test-L622			
	PSNR \uparrow	SSIM \uparrow	LPIPS \downarrow	PAUQA \uparrow
$\theta = 0$	23.82	89.93	9.19	51.33
$\theta = 0.25$	22.08	88.78	9.73	50.34
$\theta = 0.75$	23.23	89.58	9.55	51.05
$\theta = 1$	22.87	88.99	10.29	50.32
Ours	24.07	90.19	9.11	51.34

designed image-text fusion mechanism. These results collectively demonstrate that incorporating textual features is crucial for achieving high-quality image enhancement.

3) *Effect of the Masking Ratio*: We evaluated the effect of different masking ratios θ by comparing four variants of the model with θ set to 0, 0.25, 0.75, and 1. As shown in Table V, the best performance is achieved when $\theta = 0.5$ (Ours), indicating that an appropriate masking ratio effectively balances semantic learning and structural preservation. When no masking is applied ($\theta = 0$), the performance slightly drops, particularly in terms of PSNR and PAUQA, suggesting the importance of forcing semantic completion. In contrast, overly aggressive masking ($\theta = 1$) leads to performance degradation across all metrics due to the lack of sufficient visual context. These results validate that moderate masking encourages semantic-text interaction without compromising visual fidelity.

VII. CONCLUSION

We proposed PSG-UIENet, a Physics- and Semantics-guided Underwater Image Enhancement Network that combines the Retinex-based physical prior with high-level semantic cues from textual descriptions. Its architecture integrates a prior-free illumination estimator and a dual-branch U-shaped restorer with cross-attention-based fusion, enabling effective multimodal interaction and robust adaptation across

diverse underwater conditions. To support multimodal learning, we constructed LUIQD-TD, the first large-scale underwater dataset with paired images and scene-level textual annotations. We further introduced a text-guided metric, ITSS, and the associated ITSS Loss to promote semantic consistency between enhanced images and textual descriptions. Extensive experiments on five benchmark datasets demonstrate that PSG-UIENet achieves superior or competitive results compared to fifteen state-of-the-art approaches, validating the effectiveness of integrating physics-inspired modeling with language-based supervision. Future work will focus on richer textual supervision and stronger language guidance. We will explore longer and finer-grained annotations to capture nuanced semantics, develop stronger text-guided strategies where language plays a dominant role in guiding color and structure restoration, and investigate extreme settings where textual descriptions alone act as references. These directions could pave the way for reference-free multimodal enhancement. In summary, this work not only introduces a novel physics- and semantics-driven framework but also provides the first multimodal benchmark for underwater image enhancement, laying the foundation for further research in multimodal and language-driven underwater vision.

REFERENCES

- [1] K. He, J. Sun, and X. Tang, "Single image haze removal using dark channel prior," *IEEE Transactions on Pattern Analysis and Machine Intelligence*, vol. 33, no. 12, pp. 2341–2353, 2010.
- [2] P. Drews, E. Nascimento, F. Moraes, S. Botelho, and M. Campos, "Transmission estimation in underwater single images," in *Proceedings of the IEEE International Conference on Computer Vision Workshops*, 2013, pp. 825–830.
- [3] Y.-T. Peng, K. Cao, and P. C. Cosman, "Generalization of the dark channel prior for single image restoration," *IEEE Transactions on Image Processing*, vol. 27, no. 6, pp. 2856–2868, 2018.
- [4] D. Berman, T. Treibitz, and S. Avidan, "Diving into haze-lines: Color restoration of underwater images," in *Proc. British Machine Vision Conference (BMVC)*, vol. 1, no. 2, 2017.
- [5] E. H. Land, "The retinex theory of color vision," *Scientific American*, p. 108–128, Feb 2010. [Online]. Available: <http://dx.doi.org/10.1038/scientificamerican1277-108>
- [6] P. Zhuang, J. Wu, F. Porikli, and C. Li, "Underwater image enhancement with hyper-laplacian reflectance priors," *IEEE Transactions on Image Processing*, vol. 31, pp. 5442–5455, 2022.
- [7] W. Zhang, P. Zhuang, H.-H. Sun, G. Li, S. Kwong, and C. Li, "Underwater image enhancement via minimal color loss and locally adaptive contrast enhancement," *IEEE Transactions on Image Processing*, vol. 31, pp. 3997–4010, 2022.
- [8] S. An, L. Xu, I. Senior Member, Z. Deng, and H. Zhang, "Hfm: A hybrid fusion method for underwater image enhancement," *Engineering Applications of Artificial Intelligence*, vol. 127, p. 107219, 2024.
- [9] C. Li, C. Guo, W. Ren, R. Cong, J. Hou, S. Kwong, and D. Tao, "An underwater image enhancement benchmark dataset and beyond," *IEEE Transactions on Image Processing*, vol. 29, pp. 4376–4389, 2019.

- [10] C. Li, S. Anwar, J. Hou, R. Cong, C. Guo, and W. Ren, "Underwater image enhancement via medium transmission-guided multi-color space embedding," *IEEE Transactions on Image Processing*, vol. 30, pp. 4985–5000, 2021.
- [11] S. Xu, H. Qi, W. Wang, C. Huang, J. Wen, J. Dong, and X. Dong, "A semi-supervised physics-aware triple-stream underwater image enhancement network," 2025. [Online]. Available: <https://arxiv.org/abs/2307.11470>
- [12] Z. Fu, W. Wang, Y. Huang, X. Ding, and K.-K. Ma, "Uncertainty inspired underwater image enhancement," in *European conference on computer vision*. Springer, 2022, pp. 465–482.
- [13] L. Peng, C. Zhu, and L. Bian, "U-shape transformer for underwater image enhancement," *IEEE Transactions on Image Processing*, vol. 32, pp. 3066–3079, 2023.
- [14] C. Guo, R. Wu, X. Jin, L. Han, W. Zhang, Z. Chai, and C. Li, "Underwater ranker: Learn which is better and how to be better," in *Proceedings of the AAAI conference on artificial intelligence*, vol. 37, no. 1, 2023, pp. 702–709.
- [15] H. Qi, H. Zhou, J. Dong, and X. Dong, "Deep color-corrected multi-scale retinex network for underwater image enhancement," *IEEE Transactions on Geoscience and Remote Sensing*, vol. 62, pp. 1–13, 2024.
- [16] W. Chen, Y. Lei, S. Luo, Z. Zhou, M. Li, and C.-M. Pun, "Uwformer: Underwater image enhancement via a semi-supervised multi-scale transformer," in *2024 International Joint Conference on Neural Networks (IJCNN)*. IEEE, 2024, pp. 1–8.
- [17] Y. Cai, H. Bian, J. Lin, H. Wang, R. Timofte, and Y. Zhang, "Retinexformer: One-stage retinex-based transformer for low-light image enhancement," in *Proceedings of the IEEE/CVF international conference on computer vision*, 2023, pp. 12504–12513.
- [18] J. Bai, Y. Yin, Q. He, Y. Li, and X. Zhang, "Retinexmamba: Retinex-based mamba for low-light image enhancement," in *International Conference on Neural Information Processing*. Springer, 2025, pp. 427–442.
- [19] Z. Wang, A. C. Bovik, H. R. Sheikh, and E. P. Simoncelli, "Image quality assessment: from error visibility to structural similarity," *IEEE Transactions on Image Processing*, vol. 13, no. 4, pp. 600–612, 2004.
- [20] R. Zhang, P. Isola, A. A. Efros, E. Shechtman, and O. Wang, "The unreasonable effectiveness of deep features as a perceptual metric," in *Proceedings of the IEEE conference on computer vision and pattern recognition*, 2018, pp. 586–595.
- [21] E. H. Land and J. J. McCann, "Lightness and retinex theory," *Journal of the Optical Society of America*, vol. 61, no. 1, pp. 1–11, 1971.
- [22] A. Radford, J. W. Kim, C. Hallacy, A. Ramesh, G. Goh, S. Agarwal, G. Sastry, A. Askell, P. Mishkin, J. Clark *et al.*, "Learning transferable visual models from natural language supervision," in *International conference on machine learning*. PmlR, 2021, pp. 8748–8763.
- [23] Z. Liang, C. Li, S. Zhou, R. Feng, and C. C. Loy, "Iterative prompt learning for unsupervised backlit image enhancement," in *Proceedings of the IEEE/CVF International Conference on Computer Vision*, 2023, pp. 8094–8103.
- [24] R. Wang, W. Li, X. Liu, C. Li, Z. Zhang, X. Min, and G. Zhai, "Hazeclip: Towards language guided real-world image dehazing," in *ICASSP 2025-2025 IEEE International Conference on Acoustics, Speech and Signal Processing (ICASSP)*. IEEE, 2025, pp. 1–5.
- [25] S. Liu, K. Li, Y. Ding, and Q. Qi, "Underwater image enhancement by diffusion model with customized clip-classifier," *arXiv preprint arXiv:2405.16214*, 2024.
- [26] B. Lin, J. Dong, and X. Dong, "Perception-aware underwater image quality assessment: Dataset, perceptual quality scores and assessment network," *IEEE Transactions on Circuits and Systems for Video Technology*, 2025.
- [27] D. Berman, D. Levy, S. Avidan, and T. Treibitz, "Underwater single image color restoration using haze-lines and a new quantitative dataset," *IEEE Transactions on Pattern Analysis and Machine Intelligence*, vol. 43, no. 8, pp. 2822–2837, 2020.
- [28] K. Zuiderveld, *Contrast Limited Adaptive Histogram Equalization*. USA: Academic Press Professional, Inc., 1994, p. 474–485.
- [29] D. Huang, Y. Wang, W. Song, J. Sequeira, and S. Mavromatis, "Shallow-water image enhancement using relative global histogram stretching based on adaptive parameter acquisition," in *MultiMedia Modeling: 24th International Conference, MMM 2018, Bangkok, Thailand, February 5-7, 2018, Proceedings, Part I 24*. Springer, 2018, pp. 453–465.
- [30] S. Zhang, T. Wang, J. Dong, and H. Yu, "Underwater image enhancement via extended multi-scale retinex," *Neurocomputing*, vol. 245, pp. 1–9, 2017.
- [31] C. Ancuti, C. O. Ancuti, T. Haber, and P. Bekaert, "Enhancing underwater images and videos by fusion," in *2012 IEEE Conference on Computer Vision and Pattern Recognition*. IEEE, 2012, pp. 81–88.
- [32] C. O. Ancuti, C. Ancuti, C. De Vleeschouwer, and P. Bekaert, "Color balance and fusion for underwater image enhancement," *IEEE Transactions on Image Processing*, vol. 27, no. 1, pp. 379–393, 2017.
- [33] Q. Qi, K. Li, H. Zheng, X. Gao, G. Hou, and K. Sun, "Sguie-net: Semantic attention guided underwater image enhancement with multi-scale perception," *IEEE Transactions on Image Processing*, vol. 31, pp. 6816–6830, 2022.
- [34] T. Gaintseva, M. Benning, and G. Slabaugh, "Rave: Residual vector embedding for clip-guided backlit image enhancement," in *European Conference on Computer Vision*. Springer, 2024, pp. 412–428.
- [35] K. He, X. Chen, S. Xie, Y. Li, P. Dollár, and R. Girshick, "Masked autoencoders are scalable vision learners," in *Proceedings of the IEEE/CVF conference on computer vision and pattern recognition*, 2022, pp. 16000–16009.
- [36] E. Perez, F. Strub, H. De Vries, V. Dumoulin, and A. Courville, "Film: Visual reasoning with a general conditioning layer," in *Proceedings of the AAAI conference on artificial intelligence*, vol. 32, no. 1, 2018.
- [37] R. Hummel, "Image enhancement by histogram transformation," *Unknown*, 1975.
- [38] M. Yang and A. Sowmya, "An underwater color image quality evaluation metric," *IEEE Transactions on Image Processing*, vol. 24, no. 12, pp. 6062–6071, 2015.
- [39] K. Panetta, C. Gao, and S. Agaian, "Human-visual-system-inspired underwater image quality measures," *IEEE Journal of Oceanic Engineering*, vol. 41, no. 3, pp. 541–551, 2015.
- [40] Y. Zheng, W. Chen, R. Lin, T. Zhao, and P. Le Callet, "Uif: An objective quality assessment for underwater image enhancement," *IEEE Transactions on Image Processing*, vol. 31, pp. 5456–5468, 2022.

Shixuan Xu received the bachelor's degree in Engineering from Lanzhou University of Finance and Economics (LZUFE), Lanzhou, Gansu, China, in 2022. He is currently pursuing the master's degree in Artificial Intelligence at Ocean University of China. His research interests include computer vision, deep learning and image enhancement.



Yabo Liu received the Ph.D. degree in computer technology from Harbin Institute of Technology, Shenzhen, China, in 2025. From 2021 to 2025, he was a jointly supervised Ph.D. candidate by Harbin Institute of Technology and Peng Cheng Laboratory. He is currently a lecturer with the School of Artificial Intelligence, Ocean University of China, Qingdao, China. His current research interests include computer vision, transfer learning, machine learning, and multi-modal learning.



Junyu Dong received the B.Sc. and M.Sc. degrees from the Department of Applied Mathematics, Ocean University of China, Qingdao, China, in 1993 and 1999, respectively, and the Ph.D. degree in image processing from the Department of Computer Science, Heriot-Watt University, U.K., in 2003. He joined Ocean University of China in 2004. He is currently a Professor and the Dean of the Faculty of Information Science and Engineering, Ocean University of China. His research interests include computer vision, underwater image processing, and



machine learning.

Xinghui Dong received the PhD degree from Heriot-Watt University, U.K., in 2014. He worked with the Centre for Imaging Sciences, the University of Manchester, U.K., between 2015 and 2021. Then he joined Ocean University of China in 2021. He is currently a professor at the Ocean University of China. His research interests include computer vision, defect detection, texture analysis, underwater image processing and visual perception.

